



## The Significance of Adverse 3rd-Body Wear Damage in the Failure of Metal-on-Metal Bearings used in resurfacing and Total-Hip Arthroplasty

Elsissy Joseph G, Clarke Ian C\*, John Alun, Smith Evert J and Donaldson Thomas K

Department of Orthopaedics, Loma Linda University Medical Center (LLUMC), United States

\*Corresponding Author: Clarke Ian C, Department of Orthopaedics, Loma Linda University Medical Center (LLUMC), United States.

Received: July 30, 2018; Published: September 25, 2018

### Abstract

Large diameter, metal-on-metal (MOM) bearings used in total hip arthroplasty (THA) have been abandoned due to adverse wear. Commonly cited risks included excessive wear in large diameter CoCr bearings, edge-loading in steeply-inclined cups, and corrosion under modular CoCr heads. An alternative failure mechanism was suggested to be due to hip-impingement whereby the cup rim habitually creates pitting and microgroove damage in the opposing femoral head. It is to be noted that an RSA hip at impingement will risk a CoCr cup impinging on the tissues of the natural neck. In contrast, THA impingement risks a CoCr cup impinging on the metal femoral-neck. For this MOM retrieval study, we matched 12 each retrievals of total hip arthroplasty (THA) with modular CoCr heads and resurfacing arthroplasty (RSA) for study of microscopic wear damage. Anatomic RSA and THA models were developed to compare head:neck ratios, range of hip motion, and location of microgroove damage sites at impingement. The salient finding we report for the 1st time was that all RSA bearings featured arrays of large pits, typically 40 - 100 um or larger. The likely source of large metal fragments in RSA cases is suggested to be the CoCr cup impinging/subluxing on the femoral head, thereby creating microgroove damage. The circulating metal fragments becoming trapped under the cup created the basal and polar microgrooves, typically 40 - 100 um wide, and aligned under the rim profile of the cup. The abrasive power of such large circulating metal fragments was evident in the microscopic analyses in these 24 MOM retrievals. CoCr debris previously analyzed in MOM simulator and retrieval studies was typically characterized with particles sized less than 50 nm, i.e. 2,000 times smaller. The evidence of pitting and microgroove morphology proved similar in RSA and THA regardless of design differences. Our study is the 1st confirmation of the MOM wear/impingement mechanics offered in a prior study of fixed-head McKee-Farrar THA, i.e. hip impingement produces fatigue wear in CoCr components with release of large CoCr fragments, consistent with sliding/impaction mechanisms and adverse wear in MOM. With continued function these large fragments will decompose into CoCr particulates and also ionize into solution.

**Keywords:** Metal-on-Metal (MOM); Total Hip Arthroplasty (THA); Cobalt Chrome (CoCr)

### Introduction

Large diameter, metal-on-metal (MOM) bearings used in total hip arthroplasty (THA) have been abandoned due the excessive production of cobalt chrome (CoCr) debris and frequently the release of large quantities of Co and Cr ions [1-3]. Two most commonly cited risks were (1) excessive wear in CoCr bearings, and (2) corrosion under modular femoral heads [4,5]. However, detailed understanding of the underlying failure mechanisms remains unclear. Modular femoral heads in 28 to 32 mm diameters have been utilized for over 4 decades with excellent clinical results. Possibly, contemporary designs of 36 - 60 mm diameter heads changed the underlying corrosion dynamics [6]. Adverse wear in MOM bearings has frequently been attributed to edge-loading of steeply-inclined acetabular cups [7-9]. However, MOM simulator studies of steeply-inclined cups did not confirm those adverse clinical results [10-12].

Howie, *et al.* (2005) introduced an alternative failure mechanism for MOM bearings [13]. Retrieval analysis of 24 McKee-Farrar THA demonstrated large oriented wear tracks in what the authors termed "Type 4" abrasive wear. Their microscopic analysis demonstrated extrusion of large metal fragments (50 - 100 um wide) due to subsurface fatigue in the CoCr bearings. Since the femoral stems had integral CoCr heads, the authors were able to establish in-vivo component positions and noted that the very large bearing scratches were created at hip-impingement, most typically at extremes of flexion and abduction motions (Figures 1A, 2C). We examined 60 large-diameter THA for comparable wear mechanisms [14]. All were modular head designs and were retrieved with no information given regarding in-vivo positioning. As in our simulator wear studies [15,16] we were able to deduce in-vivo component positions by mapping each patient's habitual wear-patterns (Figure 2) [14]. We described large scratches that were termed

“microgrooves” to distinguish them from the “stripe” wear damage described on ceramic hip joints [17]. Microgrooves were visible at both the which base (Figures 2B, ‘basal’) and dome (‘polar’) of the modular THA heads. It was notable that when cups were placed at likely impingement positions on the femoral stems (Figure 1A), their rims precisely matched underlying basal and polar microgrooves (Figure 2C). With hindsight it is now apparent that these modular-head data confirmed the unique observations made on fixed-head McKee-Farrar retrievals [13]. The salient observation from these studies was that a CoCr cup rim could damage its mating CoCr head repetitively at impingement sites, thereby creating large microgrooves. We have also described femoral necks with impingement damage varying from cosmetic scratches to deep notches (Figure 3) [18]. Femoral neck-notching is a known risk with THA designs [18-23] but its prevalence is not determinable. Nevertheless, a notched femoral neck represents an unequivocal demonstration that THA impingement had habitually occurred at some terminal arc of motion for millions of gait cycles [13].

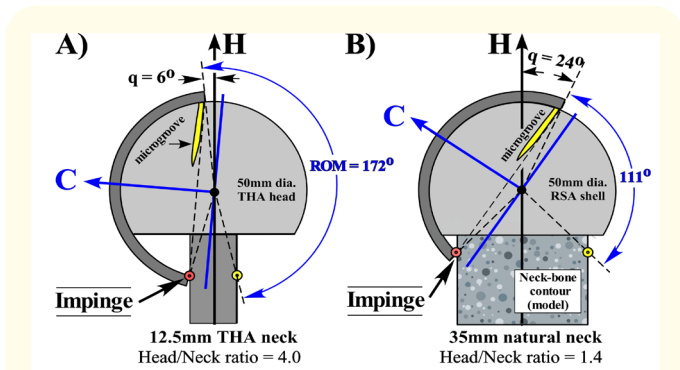


**Figure 1:** 50 mm MOM impingement models with 160°-profile cups:

(A) THA with 12.5 mm diameter neck has head: neck ratio 4.0 and ROM = 172°.

(B) RSA with 35 mm natural-neck has head: neck ratio 1.4 and ROM = 111°.

Key: C: Cup Centerline Axis; H: Head Centerline Axis; q: Angle Cup Rim makes with axis-H; ROM: Range of Motion; RSA: Resurfacing Arthroplasty; THA: Total Hip Arthroplasty.

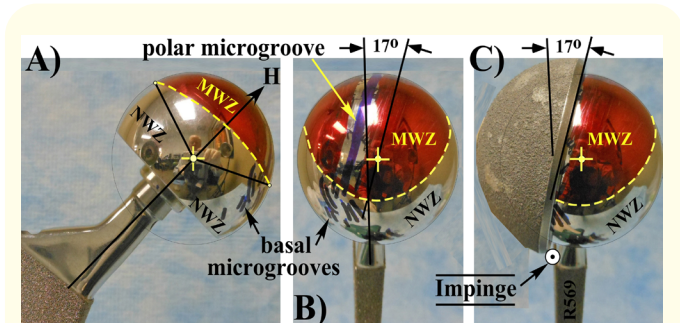


**Figure 2:** Superior main-wear zone (MWZ) stained red to differentiate from inferior non-wear (NWZ) zone. Polar and basal microgrooves stained blue and black, respectively.

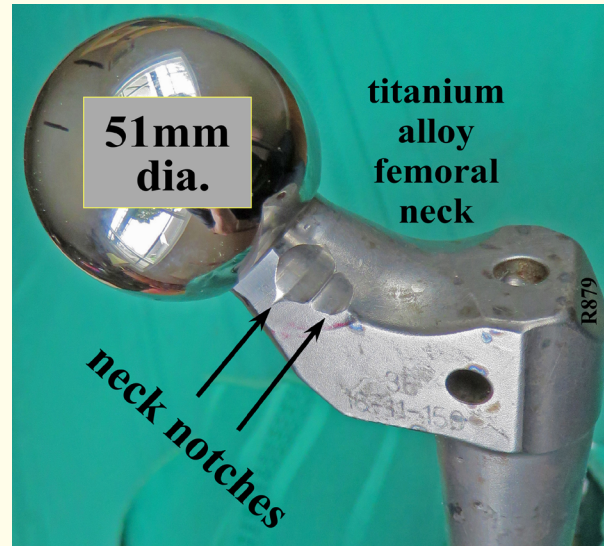


**Figure 3:** Twin notches on retrieved THA femoral-neck (titanium-alloy), 51 mm SRM case presented by permission of J. Recon. Review [Donaldson, 2015].

Resurfacing hip arthroplasty (RSA) was introduced as a more conservative alternative to the femoral resection needed with THA procedures. Alternative risks introduced with RSA concepts included, (i) retention of the larger natural neck (Figure 1A) with potential for fracture in the reamed bone, (ii) more frequent hip impingement [24] and (iii) likely more head subluxations. However, with mounting clinical experience it became apparent that RSA results were significantly better than with MOM THA [1]. It is also to be noted that RSA impingement represented metal-to-bone contact (Figure 1B). In contrast, THA impingement incurs the risk of metal-to-metal contact, thereby providing two sites for production of metal fragments (Figures 1A, 3) [13]. Therefore, to investigate the relevance of observed THA wear to RSA designs, we matched twelve each RSA and THA retrievals by vendor and diameter for our microscopic study of wear damage. Our governing hypothesis is that with THA designs repetitive impingement of the CoCr cup against a metal femoral-neck creates fatigue cracks that coalesce to form and release metal fragments [13] and with release into the joint space, the metal fragments circulate and produce adverse 3<sup>rd</sup>-body wear during gait. In contrast, RSA only risks metal-on-bone contact at impingement. Therefore hypothesis 1 is that RSA retrievals will not feature large pits created by circulating metal debris in THA. However, with RSA’s potential ROM reduced due to retention of the natural neck [24] there will be increased likelihood of the femoral component producing edge-loading of the cup rim. Thus, hypothesis 2 states that RSA cups will have larger wear areas and greater arcs of rim-loading than THA, while hypothesis 3 states that the polar microgrooves produced by the rim of the subluxing RSA cup will be positioned similar to THA, i.e. less than 40° from the head’s axis of symmetry.

**Materials and Methods**

Twelve RSA retrievals were chosen with complete patient histories and matched with 12 THA by vendor and MOM diameters (Table 1). Reasons given for revision included adverse reaction to metal debris (ARMD), pain, and cup loosening. IRB approvals were obtained for all cases. RSA and THA diameters ranged 42 to 54 mm in retrievals representative of 3 vendors. Times to revision varied generally from 10 to 76 months with one RSA outlier at 104 months. Excluding this outlier, RSA and THA cases appeared similar.

Implant Type	Diameter (mm)	Age	In Vivo (months)	Reason for Revision
RSA	42 - 54	53 (42 - 68)	58 (10 - 104)	6 ARMD, 3 Pain, 2 Loosening, 1 Infection
THA	42 - 54	61 (36 - 76)	49 (26 - 72)	10 ARMD, 1 Pain, 1 Loosening
RSA:THA Ratio	1.0	0.9	1.2	

**Table 1:** Patient demographics for two groups of explants (mean, range = min-max).

ARMD: Articular Reaction to Metal Debris.

All bearings were cleaned using a standard, non-destructive process [14,25]. Bearing geometries were assessed by contour measurement method (CMM: Legex 322, Mitotoyo, Chicago, IL). Two operators visually defined main-wear zone (MWZ) patterns on the bearings (Figure 2) and these confirmed by stereo-microscopy. Wear patterns on heads were marked with red ink and photographed, creating one polar and four orthogonal views [14,26]. The cups were similarly marked and photographed en-face, noting arcs representing edge-loading of cup rims (Figure 4). Wear patterns were measured digitally and areas calculated using standard spherical equations [14]. MWZ areas were normalized to their hemispherical bearing area, providing a hemi-area ratio for comparison across MOM diameters.

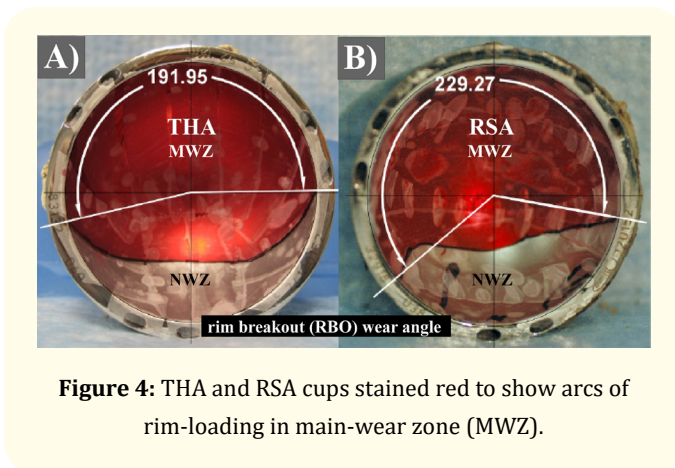


**Figure 4:** THA and RSA cups stained red to show arcs of rim-loading in main-wear zone (MWZ).

Head microgrooves were defined as polar when crossing the main-wear zone within 40° of the polar axis (Figure 2B). Equatorial microgrooves were defined at the lower boundary of the wear zone with angles greater than 40° from the polar axis. Basal stripes occurred in the non-wear zone (Figure 2: NWZ) near the base of

RSA and THA models were created to define location of microgrooves on heads at impingement. Implant range-of-motion (ROM) varies with cup rim-profile angle (p), MOM diameter, and neck width (Figure 1: t). Nearing impingement on a narrow femoral-neck, the cup rim approaches the head’s polar axis and may even cross over to the same side as the impingement site (figure 1A: rim angle-q = -6o). The RSA concept with the natural-neck limits ROM, which increases the rim-impingement angle but on the opposite side from the impingement site (Figure 1B: q = 24o). Published ROM data was used to define likely thickness (t) of natural-necks for various RSA diameters [24].

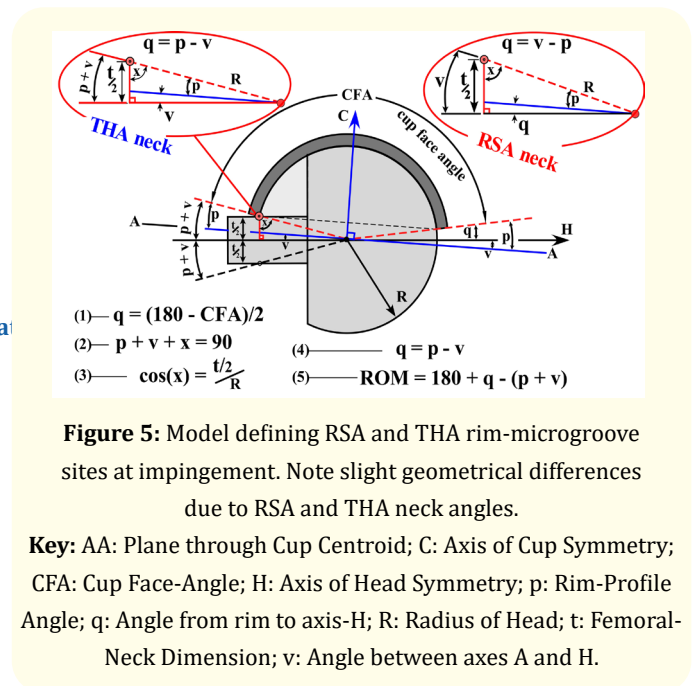


**Figure 5:** Model defining RSA and THA rim-microgroove sites at impingement. Note slight geometrical differences due to RSA and THA neck angles.

**Key:** AA: Plane through Cup Centroid; C: Axis of Cup Symmetry; CFA: Cup Face-Angle; H: Axis of Head Symmetry; p: Rim-Profile Angle; q: Angle from rim to axis-H; R: Radius of Head; t: Femoral-Neck Dimension; v: Angle between axes A and H.

the femoral heads. To aid photography, microgrooves in polar, equatorial and basal regions were stained blue, green and black, respectively, and their angulation measured relative to the axis of head symmetry. Surface roughness was analyzed by white light interferometry (WLI: NewView-600, Zygo, Tucson, AZ), each datum representing the average of 15 measurements. Microgrooves and surface pitting were analyzed by WLI and scanning electron microscopy (SEM: Zeiss MA 15, Thornwood, NY). Statistical analysis was performed using unpaired t-tests and use of boxplots.

**Results**

Analysis of RSA femoral components showed pitting defects occurred singly, in groups, and frequently as linear strings of pits. In

our WLI analysis, these measured 150 - 160  $\mu\text{m}$  wide with valley depths 5 - 10  $\mu\text{m}$  and were frequently found in proximity of microgrooves (Figure 6). These images also revealed the plowing/abrasive behavior of the presumed large metal fragments. The intersection of microgrooves demonstrated considerable plastic deformation of the rims and a similar plastic-deformation flowing onto the valley floors, the latter resembling the debris fields of avalanches (Figure 7).

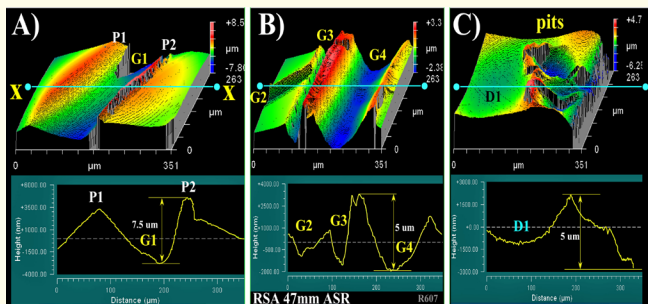


**Figure 6:** WLI images of 47 mm RSA femoral head showing pitting and microgrooves approximately 160  $\mu\text{m}$  wide with valley depths 5 - 7  $\mu\text{m}$ , A) microgroove with one side smooth and one rim sharply elevated, B) intersecting microgrooves, and C) multiple pits.

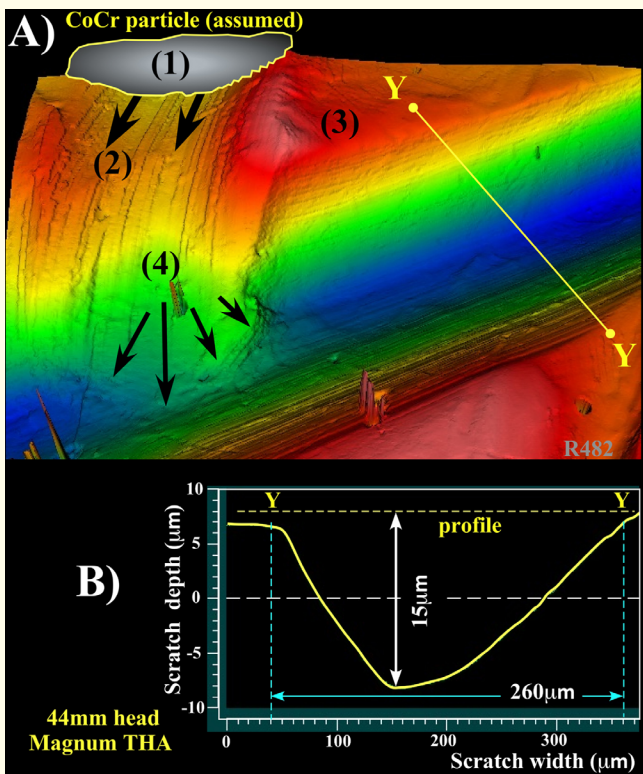


**Figure 7:** WLI imaging of intersecting microgrooves (note magnification Y-axis =  $\times 10$  x-axis),

A) Oblique 3D-view of surface contours

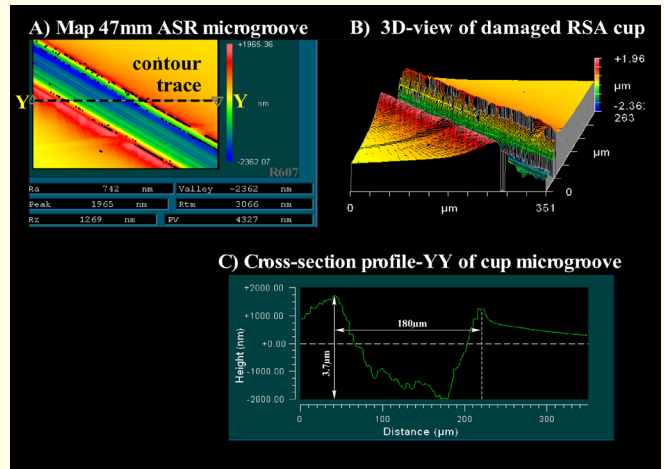
**Key for (A)**

1. Cartoon of hypothetical metal fragment
2. Longitudinal striations in microgroove-1
3. Plastically-deformed shoulder above microgroove #1
4. Avalanche appearance of cold flow confirming plowing direction of fragment penetrating microgroove-2
5. Y-Y section for microgroove-2 profile in (B)

**Key for (B)**

Y-Y cross-section profile for microgroove #2 with peak width 260  $\mu\text{m}$  and valley depth 15  $\mu\text{m}$ .

WLI imaging proved more difficult with the large diameter cups. Nevertheless, enough data was collected to show that microgrooves in cups (Figure 8) had similar topography to those in femoral heads. SEM imaging of surface damage showed a wide range of pits, demonstrating that 100  $\mu\text{m}$  width was quite a common occurrence (Figure 9). Both WLI and SEM analyses indicated there was a directionality to pitting defects, their plastically-deformed, elevated rims indicating the direction the abrading particles were travelling (Figure 9: #3). The topography of microgrooves in the basal, non-worn areas was particularly dramatic, revealing well-defined parallel striations in sidewalls (Figure 10), plastically-deformed rims (2), consistent directionality of tracking (3), and always dwarfing the size of carbide inclusions in the CoCr surfaces (4). Such microgrooves were common, whether in basal, equatorial or polar head regions, or whether on RSA or THA bearings.



**JGE Cup Scratch Zygo ASR 45mm icc18**

**Figure 8:** WLI imaging of microgrooves in RSA cup (note magnification Y-axis =  $\times 10$  x-axis).

A. Cup surface with large scratch

B. 3D-view of cup microgroove

C. Microgroove profile revealing 180  $\mu\text{m}$  between peaks, valley depth of 3.7  $\mu\text{m}$ .

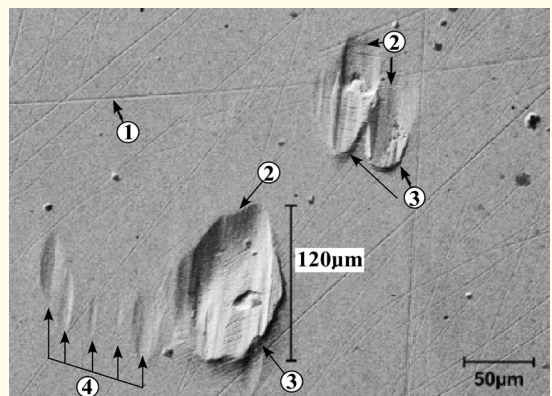


**Figure 9:** SEM images of large pits in basal zone of head.

**Key**

1. Typical background scratches in CoCr
2. Smooth terminus in defects
3. Elevated pit rims
4. Multiple shallow impact sites

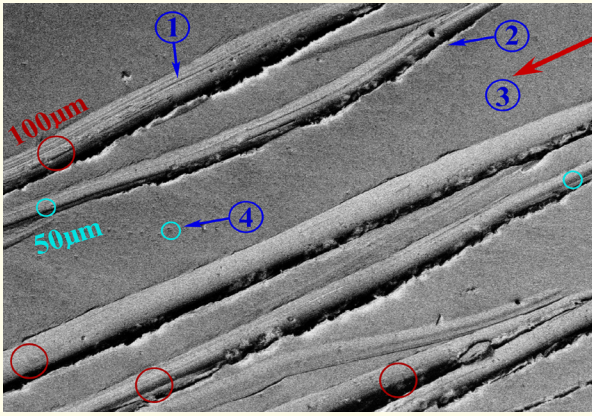


**Figure 10:** Array of basal microgrooves typically 100 µm width in RSA femoral head (43 mm ASR).

Visual and photographic study of component wear patterns revealed head main-wear zones averaged 2,061 mm<sup>2</sup> for RSA and 1,781 mm<sup>2</sup> for THA. The normalized hemi-area ratios for RSA and THA heads averaged 61% and 52%, respectively with no statistically significant difference evident (p = 0.21). With head wear patterns used for component orientation, the polar microgrooves

were shown to cross the main-wear zones with average inclinations ranging 14 - 17°. There was no statistically significant difference evident between THA and RSA bearings (p = 0.17). Equatorial microgrooves were found consistently at inferior MWZ boundaries and angulated 65o - 70° on average from the polar axis. There was no statistically significant difference evident between RSA and THA (Table 3). Basal microgrooves angulations ranged 0 - 60° with RSA and 3 - 41° with THA and these represented a statistically significant difference (Figure 10, Table 3: p = 0.005). The surface roughness data showed that basal areas on heads featured the most damage compared to polar and equatorial regions. No statistically significant difference was found between RSA and THA (Table 4: p = 0.28).

Cup wear areas averaged higher than heads, measuring 3,195 mm<sup>2</sup> for RSA and 2,026 mm<sup>2</sup> for THA but with no statistically significant difference evident between them (p = 0.43) (Table 2). The normalized hemi-area ratios averaged 78% and 59% for RSA and THA, respectively and proved to be a statistically significant difference (p = 0.01). Rim wear arcs in RSA and THA liners averaged 263° and 174° (RBO angles), respectively, giving a RSA/THA ratio of 1.5 (Table 2). This also represented a statistically significant difference (p = 0.01).

Implant Type	Head MWZ Area (mm <sup>2</sup> )	Cup MWZ Area (mm <sup>2</sup> )	Head:Cup Area Ratio	Cup RBO Angle
RSA	2061 (1085 - 3121)	3195 (1718 - 5201)	0.62	263 (167 - 360)
THA	1781 (1199 - 2541)	2026 (1420 - 4878)	0.88	174 (46 - 360)
RSA:THA Ratio	1.2	1.6		1.5
P value	0.21	0.02		0.01

**Table 2:** Diameter, Head MWZ Area, Cup MWZ Area, and RBO cup angle [Mean (min-max)].

Implant Type	Polar Stripe MOM=12	Polar Stripe Angle (q)	Equatorial Stripe MOM=12	Equatorial Stripe Angle (q)	Basal Stripe MOM = 12	Basal Stripe Angle (q)
RSA	11	17 (5 - 26)	11	65 (44 - 83)	7	29 (0 - 60)
THA	12	14 (0 - 37)	7	70 (43 - 91)	9	16 (3 - 41)
RSA:THA Ratio	0.9	1.2	1.6	0.9	0.8	1.8
p value		0.17		0.28		0.005

**Table 3:** Microgroove angles in polar, equatorial and basal regions [mean (min-max)].

Implant Type	Ball MWZ	Polar Stripe	Equatorial Stripe	Basal Stripe
RSA	22 (8 - 63)	166 (55 - 462)	393 (32 - 1868)	526 (67 - 2208)
THA	23 (5 - 63)	103 (27 - 291)	163 (25 - 388)	183 (54 - 406)
RSA: Ratio	1.0	1.6	2.4	2.9
p value	0.81	0.17	0.77	0.28

**Table 4:** Average surface roughness (Ra nm) [mean (min-max)].

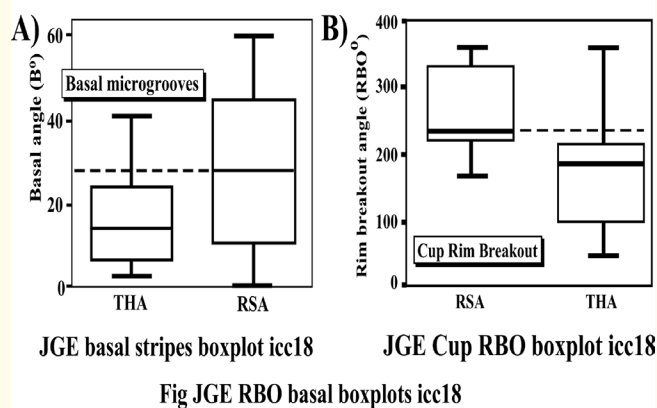


**Figure 11:** Boxplot analyses with A) arcs of rim wear (RBO), and B) basal microgroove angles.

## Discussion

We analyzed surface damage on 24 retrieved, large diameter, modular MOM bearings, looking for evidence that pitting in resurfacing arthroplasty (RSA = 12) would be minimal compared to total hip arthroplasty (THA = 12). The salient finding was that all RSA bearings demonstrated arrays of large pits, typically 40 - 100  $\mu\text{m}$  or larger. These data negated our 1<sup>st</sup> hypothesis. This unequivocal wear evidence was surprising given the noted abrasion-resistance of CoCr alloy and the fact that RSA bearings did not have the risk of metal-on-metal neck contact during impingement. Our findings indicated that the most likely source of large metal fragments came from the RSA cup impinging/subluxing on the femoral head and creating microgrooves. The 2<sup>nd</sup> surprise was the size of the pitting damage. The CoCr debris previously analyzed in MOM simulator and retrieval studies was typically characterized with particles sized less than 50 nm [27,28]. Our retrieval studies indicate that CoCr particles released in vivo were actually 2,000 times larger. This retrieval evidence demonstrated unequivocally that large circulating metal particles were impacting CoCr surfaces, sometimes producing pits and sometimes abrading the surface as in microgroove formations.

The basal microgrooves were particularly interesting. These formed in what essentially represented seldom-worn or non-worn inferior regions of femoral components. As a result of these being essentially non-wear regions, the basal surfaces retained the highest roughness score (Table 3). These data provided our new hypothesis, that basal pitting and their microgrooves represented the damage created by the ingress of circulating metal fragments. The observation that basal and polar microgrooves typically aligned under the rim profile of the cup indicated that they were part of the same damage mechanism forming at impingement.

There are many limitations in hip retrieval studies. At the beginning of study, our opinion was that potential for reduced ROM in RSA cases [24] would result in polar microgrooves with larger q-angles than RSA cases (Figure 1). The impingement models were useful for ROM and angle-q data (Figure 5) but did not differentiate between THA and RSA microgroove sites. However, the evidence that RSA femoral components featured similar polar microgroove formations as THA supported hypothesis 3. In addition, due to the small sample size it would be difficult to find differences in RSA and THA wear patterns. Even significant differences found with respect to hemi-area ratios and arcs of rim-loading in RSA cups could possibly be due to combinations of (i) surgical positioning, (ii) hip subluxation, or (iii) likelihood that RSA patients were more active than their THA counterparts. Thus, hypothesis 2 remains unproven, that RSA cups would have larger wear areas and greater arcs of rim-loading than THA.

## Conclusions

In conclusion, it is unknown under what conditions a cup rim will damage a CoCr femoral head. It is also unknown whether it is the cup rim that creates the microgrooves or the entrapped metal fragments that abrade, or both [29]. However, the destructive power of large metal fragments was made evident in these CoCr micrographs. Given these new data, our hypothesis is that the microgroove represents a wear mechanism created over millions of hip load-cycles as the cup rim oscillates on the femoral head during impingement, i.e. a sawing mechanism. The inferior performance of THA with MOM bearings may be due to this microgroove effect plus the additional risk of metal-on-metal neck impingement. Our salient finding was that the patterns of main-wear zones and morphology of microgrooves and pits were virtually identical between RSA and THA. Our study is the 1st confirmation of the wear mechanics offered in the fixed-head McKee-Farrar study [13], that hip impingement produces fatigue wear with release of large metal fragments, consistent with sliding/impaction mechanisms in MOM bearings. The basal, equatorial and polar microgrooves are also explained as impingement mechanisms producing adverse 3rd-body wear in MOM bearings.

## Bibliography

1. Karachalios T., *et al.* "Total hip arthroplasty: survival and modes of failure". *Efort Open Reviews* 3.5 (2018): 232-239.
2. Langton D., *et al.* "Early failure of metal-on-metal bearings in hip resurfacing and large-diameter total hip replacement. A consequence of excess wear". *Journal of Bone and Joint Surgery British* 92B.1 (2010): 38-46.

3. Langton DJ., *et al.* "Blood metal ion concentrations after hip resurfacing arthroplasty: a comparative study of articular surface replacement and Birmingham Hip Resurfacing arthroplasties". *Journal of Bone and Joint Surgery British* 91.10 (2009): 1287-1295.
4. Goldberg JR., *et al.* "A multicenter retrieval study of the taper interfaces of modular hip prostheses". *Clinical Orthopaedics* 401 (2002): 149-161.
5. Langton DJ., *et al.* "Taper junction failure in large-diameter metal-on-metal bearings". *Bone Joint Research* 1.4 (2012): 56-63.
6. Panagiotidou A., *et al.* "Enhanced wear and corrosion in modular tapers in total hip replacement is associated with the contact area and surface topography". *Journal of Orthopaedic Research* 31.12 (2013): 2032-2039.
7. Langton D., *et al.* "Adverse reaction to metal debris following hip resurfacing". *Journal of Bone and Joint Surgery British* 93B.2 (2011): 164-171.
8. Morlock MM., *et al.* "Modes of Implant Failure After Hip Resurfacing: Morphological and Wear Analysis of 267 Retrieval Specimens". *Journal of Bone and Joint Surgery American* 90.3 (2008): 89-95.
9. Underwood RJ., *et al.* "Edge loading in metal-on-metal hips: low clearance is a new risk factor". *Journal of Engineering in Medicine* 226.3 (2012): 217-216.
10. Angadji A., *et al.* "Influence of cup orientation on the wear performance of metal-on-metal hip replacements". *Proceedings of the Institution of Mechanical Engineers* 223.4 (2009): 449-457.
11. Clarke IC., *et al.* "Acetabular cups in 60 mm metal-on-metal bearings subjected to dynamic edge-loading with 70 degrees peak inclination in 10-million cycle simulator study". *Lubricants* 6 (2017).
12. Williams S., *et al.* "Tribology and wear of metal-on-metal hip prostheses: influence of cup angle and head position". *Journal of Bone and Joint Surgery American* 90.3 (2008): 111-117.
13. Howie DW., *et al.* "The long-term wear of retrieved McKee-Farrar metal-on-metal total hip prostheses". *Journal of Arthroplasty* 20.3 (2005): 350-357.
14. Clarke IC., *et al.* "Normal and Adverse Wear Patterns Created In-vivo on MOM Surfaces - a retrieval study representing four vendors". In: Kurtz SM, Greenwald SA, Mihalko WM, Lemons JA, ed. *Metal-on-Metal Total Hip Replacement Devices*. West Conshohocken, PA: ASTM International (2013): 157-192.
15. Bowsher JG., *et al.* "What is a "normal" wear pattern for metal-on-metal hip bearings?" *Journal of Biomedical Materials Research Part B: Applied Biomaterials* 91.1 (2009): 297-308.
16. Clarke IC., *et al.* "Simulator Model Demonstrating Intermittent Edge-loading of Steeply-inclined MOM Bearings - A Clinically-relevant Incorporation of Cup-flexion Motion". *Reconstructive Review* 7.3 (2017).
17. Esposito CI., *et al.* "Wear in alumina-on-alumina ceramic bearings. A retrieval analysis of edge loading". *Journal of Bone and Joint Surgery American* 94.7 (2012): 901-907.
18. Clarke IC., *et al.* "Risk of Impingement and Third-body Abrasion With 28-mm Metal-on-metal Bearings". *Clinical Orthopaedics and Related Research* 472.2 (2014): 497-508.
19. Donaldson TK., *et al.* "Excessive anteversion leads to failure at 3 years due to impingement as evidenced by twin notches in T16A4V stem". *Reconstructive Review* 5.2 (2015).
20. Gambera D., *et al.* "Metallosis due to impingement between the socket and the femoral head in a total hip prosthesis. A case report". *Acta Biomedica de Ateneo Parmense* 73.5-6 (2002): 85-91.
21. Iida H., *et al.* "Metallosis due to impingement between the socket and the femoral neck in a metal-on-metal bearing total hip prosthesis. A case report". *Journal of Bone and Joint Surgery American* 81.3 (1999): 400-403.
22. Incavo SJ., *et al.* "Failure of the polyethylene liner leading to notching of the femoral component in bipolar prostheses". *Orthopedic Reviews* 22.6 (1993): 728-732.
23. Leung K., *et al.* "Notching of the femoral stem neck in metal-on-metal total hip replacement: a case report". *Journal of Orthopaedic Surgery* 21.1 (2013): 113-116.
24. Bengs BC., *et al.* "Less range of motion with resurfacing arthroplasty than with total hip arthroplasty". *Acta Orthopaedica* 79.6 (2008): 755-762.
25. Clarke I., *et al.* "A new method for simulating edge-wear mechanics in THA relevant to patient gait: a ten-million cycle study with 60 mm MOM bearings". *Bone and Joint Journal* (2017).
26. Clarke I., *et al.* "What is a normal wear rate for ceramic-on-ceramic THA with clinical success spanning three decades in young and active patients?" *Bone and Joint Journal* (2017).
27. Doorn PF., *et al.* "Metal wear particle characterization from metal on metal total hip replacements: transmission electron microscopy study of periprosthetic tissues and isolated particles". *Journal of Biomedical Materials Research* 42.1 (1998): 103-111.

28. Leslie I., *et al.* "Effect of bearing size on the long-term wear, wear debris, and ion levels of large diameter metal-on-metal hip replacements-An in vitro study". *Journal of Biomedical Materials Research Part B: Applied Biomaterials* 87.1 (2008): 163-172.
29. McHugh D., *et al.* "Plastic Deformation from Edge Loading is common on Retrieved Metal-on-Metal Hips and Can Be Predicted With Finite Element Analysis". In: Kurtz SM, Greenwald SA, Mihalko WM, Lemons JA, ed. *Metal-On-Metal Total Hip Replacement Devices* (2013): 235-250.

**Volume 1 Issue 1 October 2018**

**© All rights are reserved by Clarke Ian C., *et al.***